INTERNATIONAL SOCIETY FOR SOIL MECHANICS AND GEOTECHNICAL ENGINEERING

Development of localized low permeability in heavy slurry induced by water seepage

Développement de boues lourdes localisées à faible perméabilité induites par des infiltrations d'eau

Ema Yoshikawa & Yasutaka Watanabe
Geology and Geotechnical Engineering Division, Sustainable System Research Laboratory, Central Research Institute of Electric Power Industry, Japan, yoshikawa3829@criepi.denken.or.jp

Hideo Komine & Shigeru Goto
Faculty of Science and Engineering, Dept. of Civil & Environmental Eng., Waseda University, Japan

Mitsugu Yoshimura
Engineering Division, Soil and Rock Engineering Co., Ltd., Japan

ABSTRACT: Heavy slurry developed by mixing barite powder with Na-bentonite slurry is expected to be used for water cut-off in the decommissioning process of the damaged Fukushima Daiichi Nuclear Power Station because of its low permeability. This paper presents the results of a laboratory investigation undertaken to elucidate the localization on low-permeability of the heavy slurry induced by water seepage. Heavy slurry in a column was prepared for water seepage, during which the overall flow rate was measured within an arbitrary time interval, distribution of wet density was scanned using radioisotope equipment, and water-pressure distribution was monitored by pressure sensors. After the permeability test, the column was divided into several parts to measure the hydraulic conductivity of each part. The results show that most of the parts shows dispersed state and had higher permeability than that of the entire column; the top and bottom layers showed lower permeability. The low permeability of the slurry could be attributed to the development of dense soil skeletons at the bottom layer and high montmorillonite content at the top layer.

RÉSUMÉ : Une suspension épaisse développée en mélangeant de la poudre de barytine avec une suspension de Na-bentonite devrait être utilisée pour la coupure d'eau dans le processus de déclassement de la centrale nucléaire endommagée de Fukushima Daiichi en raison de sa faible perméabilité. Cet article présente les résultats d'une étude de laboratoire entreprise pour élucider la localisation sur la faible perméabilité du lisier lourd induit par l'infiltration d'eau. Une suspension épaisse dans une colonne a été préparée pour l'infiltration d'eau, au cours de laquelle le débit global a été mesuré dans un intervalle de temps arbitraire, la distribution de la densité humide a été analysée à l'aide d'un équipement radio-isotopique et la distribution de la pression de l'eau a été surveillée par des capteurs de pression. Après le test de perméabilité, la colonne a été divisée en plusieurs parties pour mesurer la conductivité hydraulique de chaque partie. Les résultats montrent que la plupart des pièces présentent un état dispersé et ont une perméabilité plus élevée que celle de la colonne entière; les couches supérieure et inférieure ont montré une perméabilité plus faible. La faible perméabilité du lisier pourrait être attribuée au développement de squelettes de sol denses dans la couche inférieure et à une teneur élevée en montmorillonite dans la couche supérieure.

KEYWORDS: slurry; bentonite; water cut-off.

1 INTRODUCTION.

In 2011, the Tohoku Earthquake off the Pacific coast caused a serious accident at the Fukushima Daiichi Nuclear Power Station (1F). The water leakage from containment vessel have been one of the problems that should be solved to avoid radioactive exposure. Currently, as part of the decommissioning on the 1F, containment of contaminated water using the heavy slurry with high specific gravity and high fluidity is being considered (IRID, 2016). In this method, heavy slurry is filled inside the damaged part to cause clogging of the water path by soil particles and suppress the outflow of contaminated water (Yoshikawa, 2019). Figure 1 shows the heavy slurry used in this study (Yoshikawa, 2017). Heavy slurry is bentonite suspension added with barite and has been conventionally used as a drilling fluid during ground excavation. Formation of low-permeability filter cake is one of the principal functions of slurries in ground excavation to seal pores and other openings. (Darley and Gray, 1988). In previous studies, the water impermeability of the slurry after filter cake formation has been deeply evaluated (Nguyen et al., 2012). However, there are few studies on the formation process of the soil skeleton that induced by water flow, and in particular,

the behavior of the fluid part. From the safety perspective, it is necessary to have multiple-barrier functions including fluid part not only filter cake as a countermeasure against contaminated water from the radiation accident such as 1F. For example, maintain some part at dispersed state is desirable for self-repairs new damaged parts such as cracks in filter cake at the perspective of long-term decommissioning. Therefore, it is required for us to understand the development process of low permeability, by clarifying the low permeability of the entire material and investigating the relationship between the properties of each part.

The low permeability of poor ground material such as dredged soil and slurries are generally evaluated as a function of the consolidation coefficient owing to consolidation or as the hydraulic conductivity of filter cake formed at the edges. However, because heavy slurry comprises montmorillonite that expansive mineral in bentonite and non-expansive minerals such as barite, it is also necessary to examine the change in the montmorillonite content of each position for a more precise evaluation of low permeability.

In this study, assuming the use for decommissioning the 1F accident reactor, the permeability was directly evaluated by passing water from top to the heavy slurry and measuring the flow rate. In order to evaluate the changes in the properties inside

the heavy slurry during water flow, the wet density and the distribution of lateral earth pressure and pore water pressure were measured by the radioisotope (RI) sensor and pressure sensor. In addition, to evaluate the distribution of water impermeability in the water flow direction, the specimen after constant water flow was divided and a hydraulic conductivity test was performed for each layer. Thereafter, a solid phase analysis of each layer was performed.

2 MATERIALS AND METHOD

2.1 Heavy slurry

Heavy slurry is used as a ground stabilizer for ground excavation, and is characterized by a high specific gravity in the range of 1.1 to 2.0. The heavy slurry used in this study was prepared by dispersing 10 g of Na-type bentonite and 140 g of barite into a 0.2 wt.% aqueous solution of sodium pyrophosphate. In this study, two tests were carried out using the above-mentioned heavy slurry with a specific gravity of 1.8.

Figure 1. Heavy slurry

2.2 Test method

2.2.1 Column test with RI scan and pressure measurement

Figure 2 is a schematic diagram of a column test with the radioisotope (RI) density scanning system. In this test, a transparent acrylic column with a height of 1000 mm, an inner diameter of 200 mm, and a thickness of 5 mm was filled with a heavy slurry up to the initial specimen height, L_0=750 mm, and water was supplied from the top surface and drained from the bottom. A Marriott siphon was used to maintain a constant water level at a position 1515 mm high from the drainage surface. The flow rate was evaluated by measuring the weight of the water sampling container with an electronic balance at regular intervals. The water sampling container was installed with a minimum opening in the drainage section to satisfy the atmospheric pressure.

In order to evaluate the development of inhomogeneity caused by water flow inside heavy slurry, the time course of wet density distribution was measured by in-column density scanning (hereinafter referred to as density scanning) using ^{60}Co as a radiation source. In the density scanning, a downward scanning was performed at a constant speed using a radiation source, measured the transmitted dose of radiation. Simultaneously, the changes in the lateral earth pressure distribution and pore water-pressure distribution with respect to time were measured. For the pressure measurement, a lateral earth pressure gauge and a pore water-pressure gauge were installed on the side surface of the acrylic column such that they were perpendicular to the radiation transmission path, and measurements were taken at five points in vertical directions.
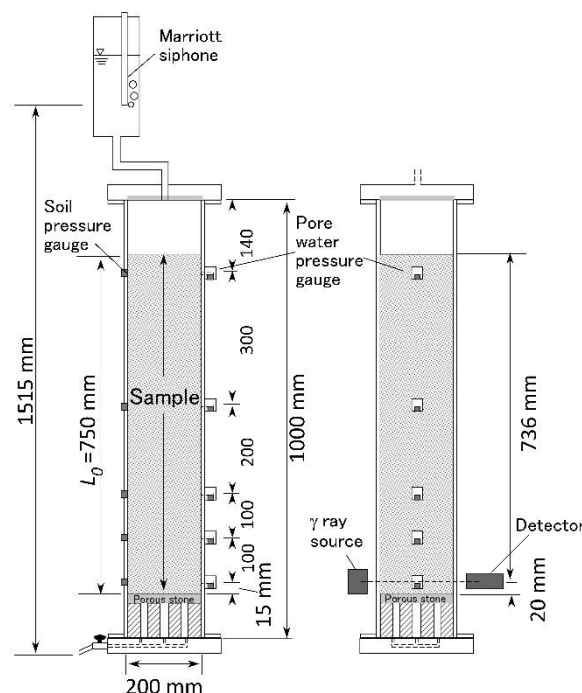

Figure 2. Column for radio isotope scan and pressure measurement

2.2.2 Constant head permeability test

Figure 3 is a schematic diagram of the constant head (CH) permeability test. In this test, the specimen after the permeability test was divided in the vertical direction, and the permeability test was performed on each layer. Figure 3 (a) is a schematic diagram of the permeability test. The mold is made up of transparent acrylic with a structure that can be divided into five layers every 30 mm. A perforated acrylic plate and a membrane filter with 0.25 x 0.075 μm pore diameter were installed at the top and bottom of the specimen. The internal dimensions of the mold before division measured as 150 mm in height and 60 mm in diameter. Water was passed from the upper surface of the specimen at a constant water level with a head difference of 540 mm. When preparing the specimen, the uniformly stirred slurry was poured in, and the air entrained during filling was discharged using a glass rod. For water sampling, a water sampling bottle with a minimum opening to satisfy the atmospheric pressure condition was used to prevent evaporation during the permeability test. The flow rate was evaluated by measuring the mass of the water sampling bottle with an accuracy of 0.1 mg at any time after the start of the water flow. The initial height L_0 of the specimen was 150 mm, and the hydraulic conductivity was calculated by Eq. (1) and (2) using the height L that changes during the test. The average hydraulic gradient i of the entire specimen was 3.6 to 4.0 with the change of the specimen height L.

$$k_T = \frac{L}{h} \times \frac{Q}{A(t_2 - t_1)} \tag{1}$$

$$k_{15} = k_T \cdot \frac{\eta_T}{\eta_{15}} \tag{2}$$

where k_T is the hydraulic conductivity (m/s) at laboratory temperature T (°C), k_{15} is the hydraulic conductivity (m/s) at 15 °C, L is the actual specimen height (m) in the direction of flow, Q is the water discharge volume (m^3), A is the specimen cross-section area (m^2), t_2-t_1 is the time difference (s), h is the hydraulic head difference (m), and η_T/η_{15} is the ratio of the coefficient of dynamic viscosity of water at 15 °C.

To identify the layers that predominate the overall permeability

of the slurry, each vertical layer of the specimen was divided after the permeability test. The hydraulic conductivity of each layer was measured independently using the same method as above. Figure 3 (b) presents a schematic diagram of the permeability test after dividing each layer. Figure 4 illustrates the procedure for dividing the specimen. After the flow rate converged to a certain value in the permeability test for the entire specimen, the mold was divided into five 30-mm-thick layers in the top-down direction to avoid disturbing the state of the specimens. A 0.5-mm-thick steel plate, covered with a pre-saturated 0.25 x 0.075 µm pore diameter membrane filter with the hydraulic conductivity of more than 1.1×10^{-5} m/s (Watanabe and Tanaka, 2016), was inserted into the separation part of the mold. Subsequently, the upper and lower filter covering the steel plate were separated. A top and base cap were set on each divided layer and wrapped by the membrane filters to create each divided specimen. The hydraulic head difference was adjusted so that the hydraulic gradient was the same (i=3.6) for each divided layer. The hydraulic conductivity of each layer after the division was measured over a shorter elapsed time during 10-30 min after flushing so as not to affect the sample properties. The method for calculating the hydraulic conductivity, and countermeasures to prevent evaporation follows that for permeability tests depicted as Figure 3 (a). The hydraulic conductivity of each layer after the division was synthesized as equivalent hydraulic conductivity, k_v, and compared with the hydraulic conductivity before division. Equivalent hydraulic conductivity, k_v, was calculated using Eq. (3).

$$k_v = \frac{L}{\frac{l_1}{k_1} + \frac{l_2}{k_2} + \cdots \frac{l_n}{k_n}} \qquad (3)$$

where k_v is the equivalent hydraulic conductivity (m/s), l_n is the actual n-th layer height (m), and k_n is the measured hydraulic conductivity of the n-th layer (m/s).
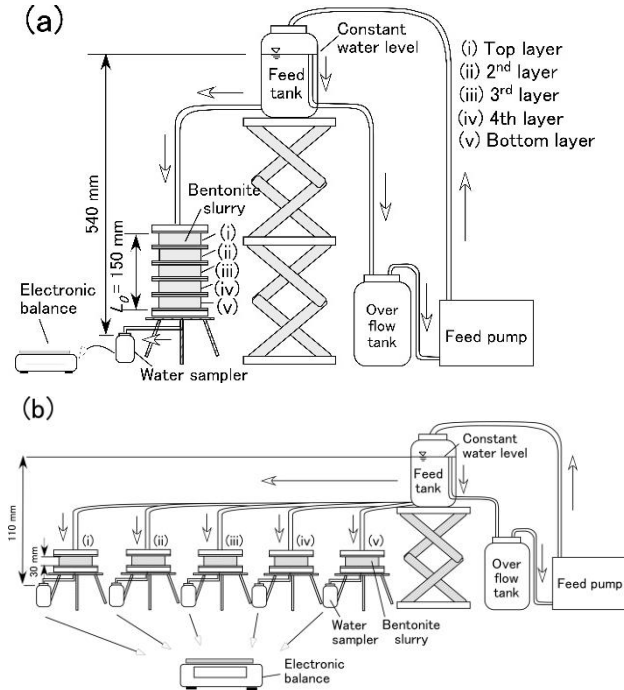

Figure 3. Schematic of constant head (CH) permeability test, (a) permeability test and (b) permeability test after dividing each layer (divided CH)
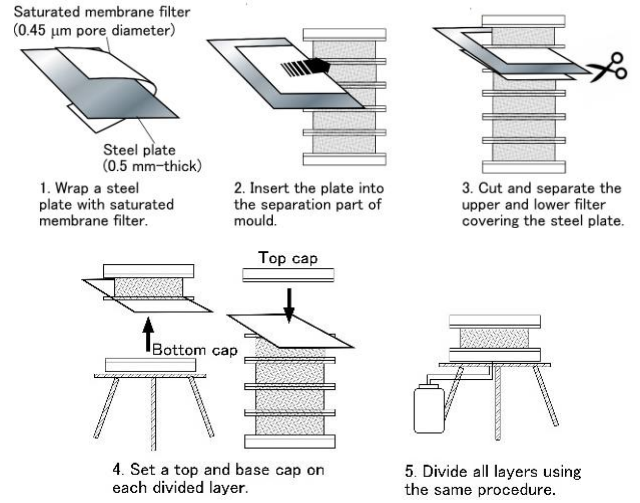

Figure 4. Procedure for dividing the specimen

After conducting the permeability test, the uppermost layer was freeze-dried, and then its structure was observed using an electron microscope. In addition, some analyses were conducted for each layer to evaluate the distribution of montmorillonite, which contributes to the development of low permeability. A methylene blue adsorption test (JIS Z 2451) was conducted for each layer to evaluate the distribution of montmorillonite. Mixed ratio of barite was evaluated by measuring average particle density in each layer. The effective montmorillonite dry density (EMDD), which indicates the abundance of montmorillonite in each part, was calculated using Eq. (4), (5) and (6).

$$\rho_{em} = \frac{m_m}{V_a + V_w + V_m}$$
$$= \frac{\rho_b C_m}{100 - \rho_b (100 - C_m)/\rho_{nm}} \qquad (4)$$

$$\rho_b = \frac{\rho_d (100 - R_{ba})}{100 - \rho_d R_{ba}/\rho_{ba}} \qquad (5)$$

$$\rho_{nm} = \left(1 - \frac{C_m}{100}\right) \frac{\rho_{sb}}{1 - C_m/100 \cdot \rho_{sb}/\rho_m} \qquad (6)$$

where ρ_{em} is the EMDD (Mg/m^3), m_m denotes the montmorillonite mass (Mg), V_a, V_w, and V_m denote air, pore water, and montmorillonite volume (m^3), respectively, C_m denotes montmorillonite content (%), ρ_b denotes effective clay density (Mg/m^3), ρ_{nm} denotes the average particle density of the accessory minerals in bentonite, ρ_d denotes dry density (Mg/m^3), R_{ba} denotes mixed ratio of barite (%), ρ_{ba} denotes particle density of barite (Mg/m^3), ρ_{sb} denotes particle density of bentonite and ρ_m denotes particle density of montmorillonite (2.78 Mg/m^3) (White and Mitchel, 1979).

3 STATE AND PERMEABILITY OF HEAVY SLURRY

3.1 Flow rate in heavy slurry

The water impermeability of the entire heavy slurry was evaluated based on the flow rate calculated from the amount of drainage. Figure 5. shows the time change of the flow rate per unit volume of the specimen with the initial height of 750 mm in Figure 2, and the specimen with the initial height of 150 mm in Figure 3 (a). As shown in Figure 5, the flow rate decreased sharply immediately after the start of water flow, and gradually decreased in approximately 50 h. The flow rate for the specimens

with L_0 = 750 mm and 150 mm almost converged after 200 and 300 h, respectively. In the column test, the height of the initial specimen was five times and the hydraulic head difference was about 2.8 times than in the permeability test; however, there was no significant difference in the downward tendency of the flow rate and the convergence value.

3.2 *Properties distribution*

Figure 6 shows the change of the wet density distribution of heavy slurry measured by density scanning. At the top, the height of the specimen decreased as water flowed from above, whereas the density at the top of the specimen increased. At the bottom, the wet density increased from 1.8 Mg/m³ in the initial state to about 2.1 Mg/m³ with the passage of time. In addition, the thickness increased in the part where the wet density increased with time. On the other hand, in the middle part ranging from a height of 100 mm to 700 mm, there was no measurable change in wet density after 332 h of water flow.

Figure 7 shows the change in the wet density at the bottom with respect to time. At 20 mm height from the lower end, the wet density increased sharply 25 h after the start of water flow, and after 60 h, the increasing tendency gradually changed, which converged to ~2.07 Mg/m³ in 200 h approximately. At 50 mm height from the lower end, the wet density increased sharply after 150 h, and converged to ~1.94 Mg/m³ in 250 h approximately. In this way, the increase in density that occurs at the bottom has a time lag depending on the height.

Figure 8 shows the changes over time in the pressure distribution inside heavy slurry. In Figure 8 (a), the lateral earth pressure showed a linear distribution from the start of water flow. After 67 h, a decrease in lateral earth pressure was measured at the bottom of the drainage section. In Figure 8 (b), the pore water pressure showed a linear distribution from the start of water flow. After 67 h, the decrease in pore water pressure at the bottom was measured. As shown in Figure 8 (c), the difference between the lateral earth pressure and the pore water pressure was almost negligible in the range of 0 kPa to 1 kPa from the start of water flow indicating that, the dispersed state was maintained. After 67 h, the difference gradually increased at the bottom, suggesting an onset of effective stress, that is, the formation of the soil skeleton at the bottom (drainage) and the increase in its thickness.
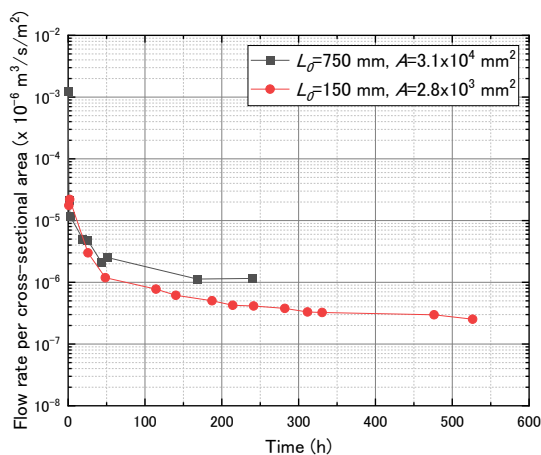
3.3 *Permeability distribution*

In order to evaluate the water impermeability development mechanism of heavy slurry, the permeability of each vertical layer was compared. Because the thickness of the uppermost layer was different from that of the other divided layers owing to the subsidence of the specimen caused by water flow, the hydraulic conductivity of each layer was compared. Figure 9 shows the time change of the hydraulic conductivity before and after the division. From Figure 9 it is clear that the values of the 2nd, 3rd, and 4th layers were larger than the average hydraulic conductivity before division. On the other hand, in the top layer and the bottom layer, the hydraulic conductivity before the division was smaller than that of each other layer.
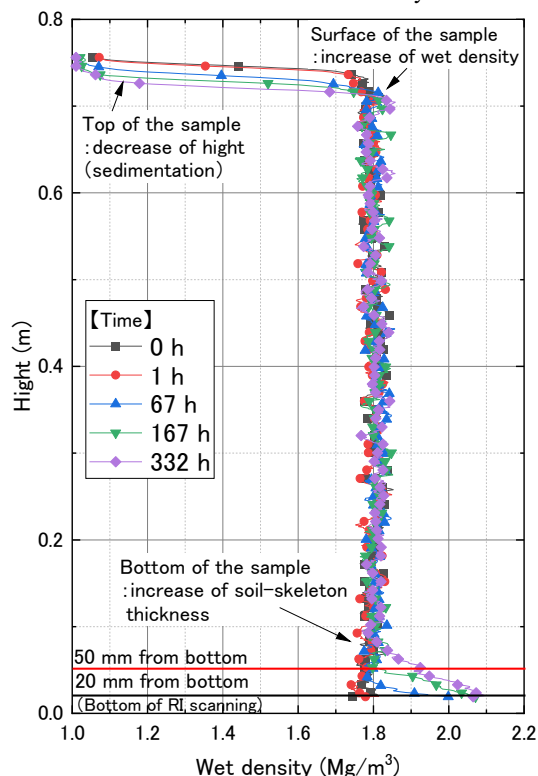

Figure 6. Wet density distribution of heavy slurry measured by RI density scanning

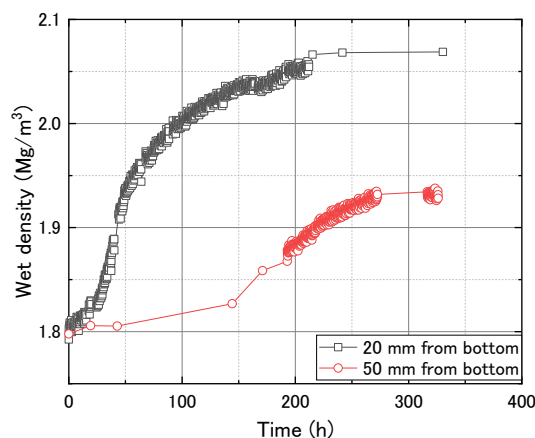Figure 5. flow rate of heavy slurry in CH permeability test and Column test

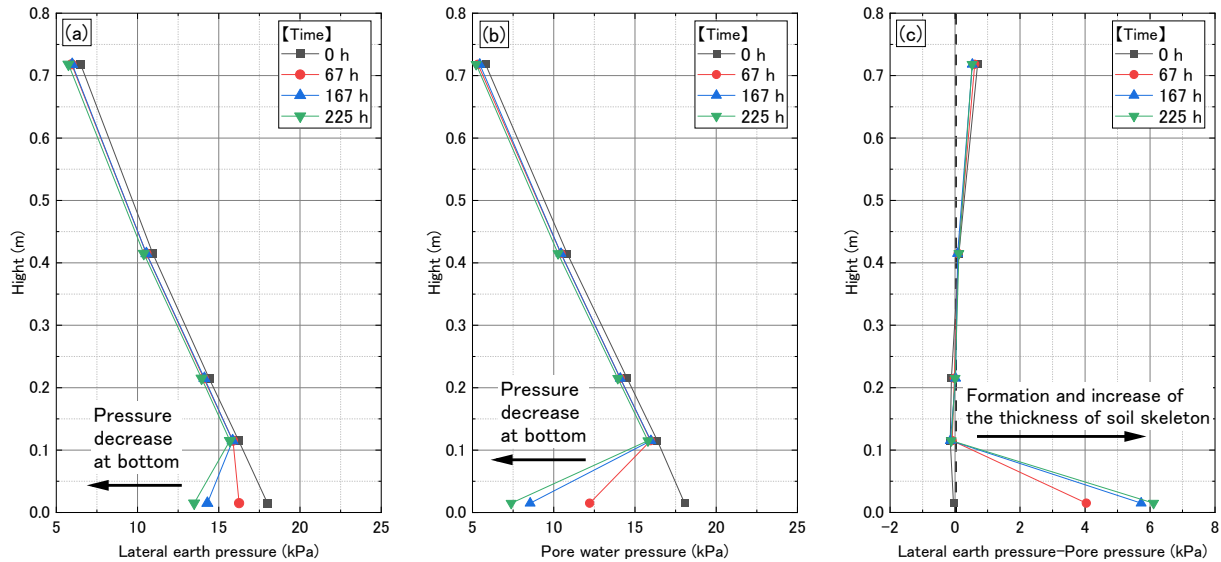Figure 7. Change over time in the wet density at the bottom

Figure 8. Pressure distribution in heavy slurry

The combined value of the hydraulic conductivity of each layer was equal to the hydraulic conductivity of the entire specimen before division. Therefore, the hydraulic conductivity measured for the entire slurry is considered to be the composite value of layers with different hydraulic conductivity, that is, the equivalent hydraulic conductivity.
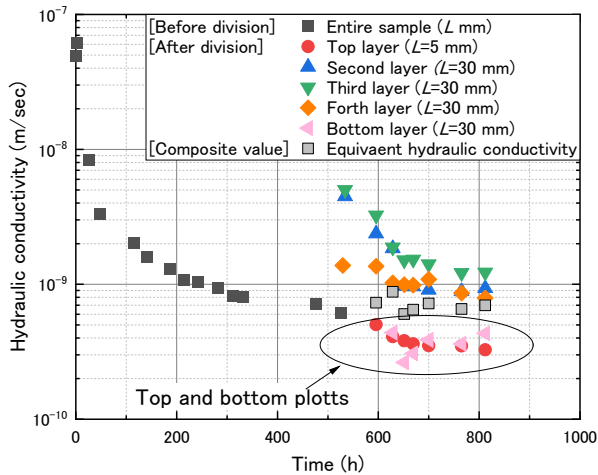

Figure 9. Hydraulic conductivity of heavy slurry before and after the division

3.4 *Analysis and discussion*

In order to observe the structure of the specimen, the top layer of the specimen (Figure 3, specimen (i)) after the divided permeability test was freeze-dried, and then observed with an electron microscope. Figure 10 (b) shows a vertical cross-sectional photograph of the uppermost layer after freeze-drying. Figure 10 (c) shows an electron microscopic image of the sample taken from each position. The difference between the two layers with different color tones was observed in the uppermost layer after analysis of the permeability test under an electron microscope. The upper part of the uppermost layer was in a state where very thin flakes regularly and densely overlapped. On the other hand, the lower part of the uppermost layer was a group of particles thought to be barite powder with a particle size of 1 to 10 μm approximately.

Figure 11 shows the distribution of the EMDD calculated from the amount of methylene blue adsorbed on the specimen after the divided permeability test. The EMDD was significantly higher in the top layer. In addition, the values for the layers below the second layer were smaller than the initial values.

As described above, in the uppermost layer, aggregates of flaky particles were observed under an electron microscope, and the EMDD was remarkably high. Therefore, in the uppermost layer of heavy slurry, it suggested that a concentrated layer of montmorillonite was formed by the sedimentation of the barite and accessory minerals.

From the results in this study, it is expected that different water-impervious development processes occurred in each part of the heavy slurry specimen. After the start of water flow, different processes such as soil skeleton formation, thickness increase, and density increase occurred in the drainage section at the bottom, according to the water permeation pressure. As a result, the water impermeability of heavy slurry is considered to have developed rapidly. On the other hand, in the uppermost part, stenosis in barite and bentonite settled inside the heavy slurry owing to the difference in specific gravity and particle size of soil particles, and montmorillonite was concentrated in the upper part. It is considered that the concentrated montmorillonite formed flocs by electrical bonding and clogged the barite in the middle part, which contributed to the development of low permeability in the upper part. In the middle part, the movement of soil particles hardly occurred maintaining the dispersed state, that is, the fluid state.

As described above, heavy slurry formed a three-layer structure consisting of a low-permeability layer in the upper part, a fluid layer in the middle part, and a low-permeability layer in the lower part as the water flowed from top to bottom. The low permeable layer was formed at the boundary between the heavy slurry and the liquid through which water passed. Therefore, we consider a high possibility that it is difficult for the water to permeate into the middle part of the heavy slurry passing through the liquid. In addition, as shown in Figure 6 and Figure 8, most of the heavy slurry remained in a fluid state even when water flowed through. Therefore, if the soil skeleton of the drainage part is cracked, it is expected that the low permeability will be restored by supplying the soil particles from the fluid part. Thus, by experimentally evaluating the development process of water impermeability of heavy slurry, it was shown that the use of heavy slurry is effective as a countermeasure against contaminated water seepage. From the above, the mechanism of water impermeability development of heavy slurry by water flow from top to bottom was clarified, and the evaluation method for water impermeability was shown.
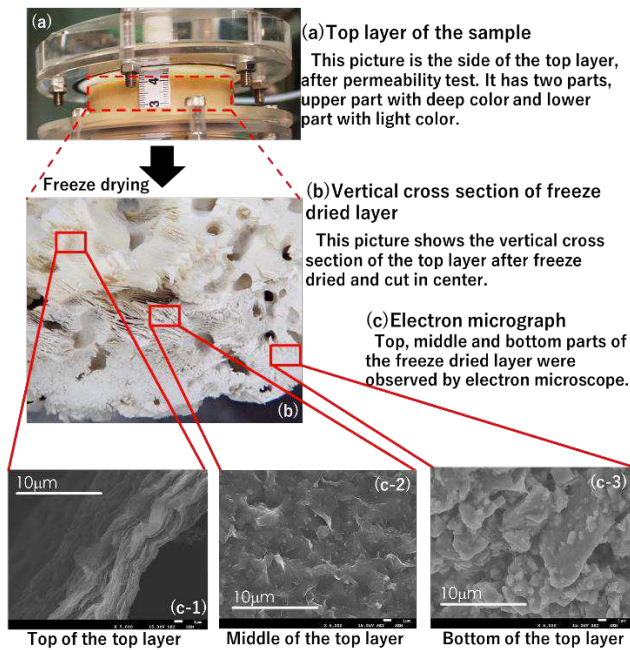
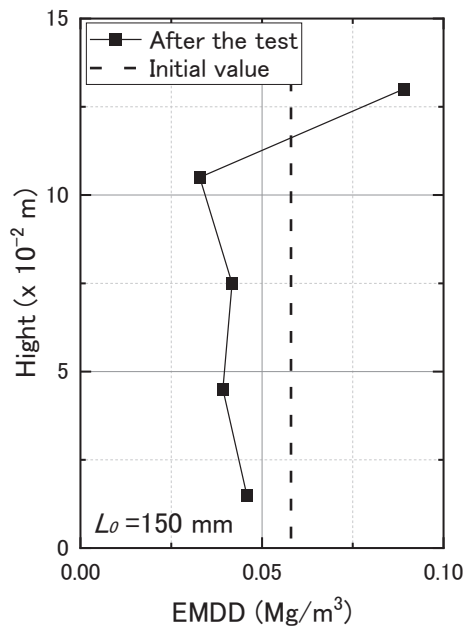Figure 10. Photos and electron micrograph of freeze-dried top layer on the permeability test

Figure 11. Distribution of effective montmorillonite dry density (EMDD)

4 CONCLUSIONS

In this study, in order to evaluate the water impermeability of heavy slurry, water was injected from the top of the material, the flow rate was measured, and the property change was evaluated. The main findings of this study are:

- The flow rate indicating the permeability of heavy slurry decreased sharply from the initial stage of water flow and converged to a constant value over time.
- The hydraulic conductivity of each layer in the water flow direction of heavy slurry was as low as about 4.0×10^{-10} m/s in the uppermost layer on the water supply side and the lowest layer on the drainage side.

- The formation of a soil skeleton in the drainage area simultaneously with the rapid development of low permeability in the early stage of water flow was confirmed. In addition, as the thickness of the earthen skeleton increased, the wet density gradually increased. On the other hand, montmorillonite, which contributes to developing low permeability was concentrated in the upper part of the specimen.

6 REFERENCES

Darley, H.C.H., Gray, G.R (1988) *Composition and properties of drilling and completion fluids, 5th edn*., Gulf Professional Publishing, Houston, TX, USA.

IRID (International Research Institute for Nuclear Decommissioning) (2016) Development of repair technology for reactor containment leak point (PCV lower part repair). Outline and problems of vent pipe water stop and S / C filling water stop. pp. 1-44.

JIS (Japanese Industrial Standard committee) (2019) Test method for methylene blue adsorption on bentonite and acid clay. JIS Z 2451.

Nguyen, T.B., Lee, C., Lim, J., Choi, H. (2012) Hydraulic characteristics of bentonite cake fabricated on cutoff walls, *Clays and Clay Minerals* 60(1): 40-51, https://doi.org/10.1346/CCMN.2012.0600104.

Watanabe Y, Tanaka Y (2016) Steady state of permeation and water chemistry of bentonite in permeability test. *In proceedings of 51th annual conference of Japanese Geotechnical Society*, pp. 897-898. [in Japanese)]

Yoshikawa, E. et al. (2019) Evaluation of properties of soil-based filling material for radiation shielding and water sealing, *16th ARC*, S15-003_JGS-088.

Yoshikawa, E. et al. (2017). The Evaluation for Radiation Shielding Ability of the Soil Materials and Application to Design for Construction, *19th ICSMGE*, 3479-348.

White, D. and Michael, G. P. (1979) A proposed method for the determination of small amounts of smectites in clay mineral mixtures, *Proc. Br. Cerm. Soc.*, 28, pp. 137-145.